Design of a low-current shunt-feedback transimpedance amplifier with inherent loop-stability.

M. Mathew, B.L. Hart and K. Hayatleh

School of Engineering, Computing and Mathematics, Oxford Brookes University, Wheatley Campus, Wheatley, Oxford, OX33 1HX, U.K.
maryashok@hotmail.com

Design of a low-current shunt-feedback transimpedance amplifier with inherent loop-stability.

Abstract

In this paper we propose a new architecture for enhancing the performance of a transimpedance amplifier (TIA) used for low-currents, and in particular, that used in biosensing. It is usually the first block in biomedical acquisition systems for converting a current in the nanoampere and picoampere range into a proportional voltage, with an amplitude suitable for further processing. There exist two main amplifier topologies for achieving this, current-mode and shunt-feedback mode. This paper introduces a shunt-feedback amplifier that embodies current-mode operation and thereby offers the advantages of both existing schemes. A conventional shunt-feedback amplifier has a number of stages and requires compensation components to achieve stability of the feedback loop. The exemplary circuit described is inherently stable because a high gain is effectively achieved in one stage that has a dominant pole controlling the frequency response. Exhibiting complementary symmetry, the configuration has an input port that is very close to earth potential. This enables the configuration to handle bidirectional input signals such are as met with in electrochemical ampero-metric biosensors. For the 0.35µm process adopted and ±3.3V rail supplies, the power dissipation is 330µW. With a transimpedance gain of 120dBohm the incremental input and output resistances are less than 2ohm and the -3dB bandwidth for non-optical input currents is 8.2MHz. The input referred noise current is 3.5pA/√Hz.

Keywords: Transimpedance amplifier; current to voltage conversion; low input impedance; shunt feedback; biosensing; complementary symmetry

1.Introduction.

A TIA is used in analogue signal processing when a current signal from a sensor is required in voltage form. Sensors are used in a wide range of applications and to set this paper in context, a number of these are listed as references in [1-5]. Various types of biosensors are available, depending on the method of signal acquisition. Among them optical biosensors are the most common. These comprise a bio-recognition sensing element integrated with an optical transducer system [6]. The optical biosensor produces a signal which is proportionate to the concentration of the measured analyte. Then an analogue front-end is required which usually incorporates a transimpedance amplifier (TIA) to convert the current signal to a proportional voltage for further processing in subsequent stages.

Usually, front-end TIAs for optical sensing are designed using a shunt-feedback [7-9], or a current-mode [10] topology. Some of the basic requirements for a TIA design are high gain, good linearity, low-noise and sufficient bandwidth for amplifying a range of biological signals. By achieving a very low input impedance, the TIA can reduce the effects due to the photodiode parasitic capacitance that may limit the bandwidth [11]. In current-mode TIAs, common-gate stages are usually used to achieve low input impedances. In basic shunt-feedback topologies, which use a voltage amplifier with a feedback network, the input impedance is decreased by the open-loop gain of the voltage amplifier. Current-mode topologies are stable and provide wide bandwidth. However, they have a higher input-referred noise current. The shunt-feedback topologies have comparatively lower input-referred noise current. In this paper, incorporating the benefits of both the topologies, we propose a topology which gives a better performance than the current-mode and conventional shunt-feedback topologies.

The proposed TIA is designed with a single-stage high transimpedance current-to-voltage amplifier with shunt-feedback. The design exhibits complementary symmetry about earth potential and therefore benefits from having an input that is very close to earth. It also has low input and output impedances (in the low-ohmic region), high transimpedance gain from a single stage and low input-referred noise current. Furthermore, in this design no compensation components are necessary to ensure frequency stability of the feedback loop as it offers inherent stability, for a wide range of feedback resistors.

2. Circuit architecture and analysis

The first part of this section considers notable points in the architecture, the second part is a circuit analysis from first principles.

The proposed circuit shown in Fig.1 comprises five interconnected vertical branches (B1-B5). A complimentary grounded-gate input stage forms the input port X to the shunt-feedback amplifier and provides a low incremental input resistance. The input current $i_{i,}$ at X, to the amplifier is $(i_s - i_f)$ where i_s, i_f are respectively, the signal current being monitored and the feedback current supplied for the amplifier output voltage v_o at Y. It is shown below that, to a high degree of predictability, $v_o = -R_F i_s$.

The DC currents I_1, I_2 in branch B1 determine the bias current, I_B, in each of the following stages. Then if I_1=I_2 and M_3, M_{10} and M_4, M_{11} are well-matched pairs, the bias current I_B in branch B_2 is equal to I_2 and X is at, or very near, earth potential in the absence of a signal current. However, this is only true if the gate-drain voltage of M_{10} is the same as that of M_3 and that of M_{11} the same as that of M_4. To help ensure this, both M_{10} and M_{11} are doubly cascoded.

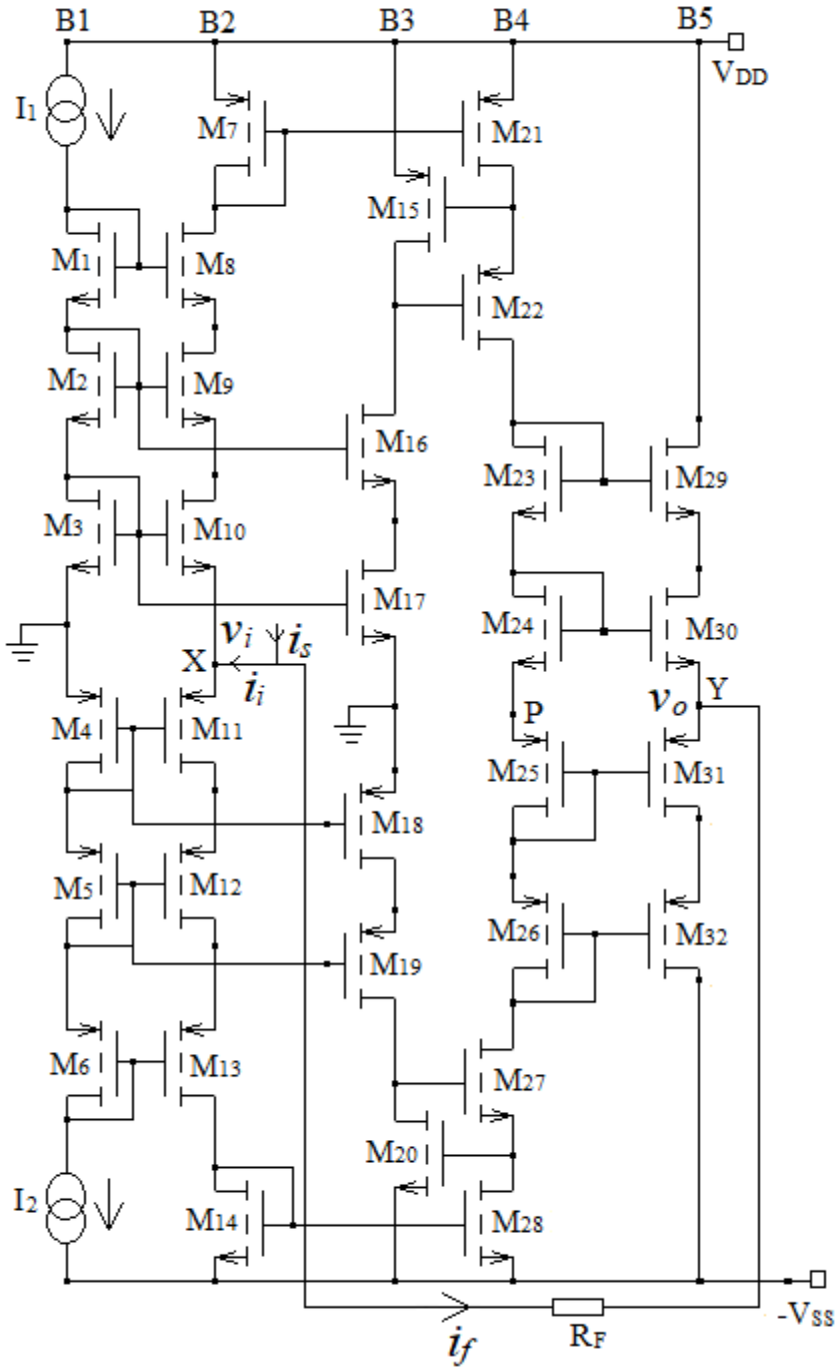

Fig.1. Proposed new Transimpedance Amplifier Circuit.

Signal current, $i_{s,}$ causes a change in the currents of M_7 and M_{14}, which are the input mosfets to the complementary regulated cascodes (RGCs) formed by M_{15}, M_{21}, M_{22} and M_{20}, M_{28}, M_{27}. Amplifying transistors M_{15}, M_{20} are supplied with drain-current loads to maximize their voltage gains and thus maximize the output resistances at the

drains of M_{22} and M_{27}. The voltage change, at point P, due to i_s appears at X via the complementary source-follower formed by M_{24}, M_{30} and M_{25}, M_{31}. These pairs are cascoded to ensure that the DC voltage at X is close to that at P.

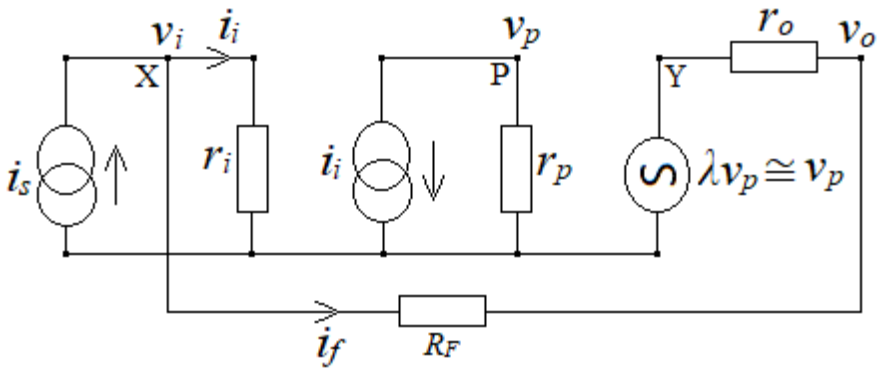

Fig.2 Small-signal low-frequency equivalent circuit of Fig.1

The points X, P, and Y of Fig.1 are shown on the corresponding small-signal low-frequency equivalent circuit of Fig.2, which serves for a circuit analysis from first principles: r_i and r_o are respectively, the incremental input resistance at X and the output resistance at Y in the absence of feedback; r_p is the incremental resistance looking in at point P; and, λ is the voltage gain of the source-follower.

There is no loss in principle, and no significant loss in accuracy in a first-order analysis, in making three simplifying assumptions. First, the current-mirrors have a current transfer coefficient of precisely unity, and second that all the N-channel mosfets have a common value, $g_{mn}$of transconductance and r_{on} for output resistance. The corresponding common values for P-channel mosfets are g_{mp},r_{op}. The third assumption is that λ=1.

$$\text{At X}, r_i = \frac{1}{(g_{mn}+g_{mp})} \tag{1a}$$

$$\text{Similarly, at Y}, r_o = \frac{1}{(g_{mn}+g_{mp})} \tag{1b}$$

When i_s, is applied, flowing in the direction shown, the input voltage v_i is given by

$$v_i = \frac{i_i}{(g_{mn}+g_{mp})} \quad (2)$$

The resultant current change in M_{11} is $g_{mp}v_i = \frac{g_{mp}i_i}{(g_{mn}+g_{mp})}$ and that in M_{10} is $-g_{mn}v_i = \frac{-g_{mn}i_i}{(g_{mn}+g_{mp})}$. Following subsequent current-mirror action, these combine to form a current i_i, that produces a voltage change $v_p = -i_i r_p$, at P.

From [12], we can write,

$$r_{p=}\left[r_{op}\left(g_{mp}r_{op}\right)^2 || [r_{on}(g_{mn}r_{on})^2]\right] \quad (3)$$

The open-circuit voltage of the source-follower is v_p assuming $\lambda = 1$.

By inspection, $v_i - v_p = i_f(R_F + r_o)$, (4)

Or, $i_i r_i - \left(-i_i\, r_p\right) = i_f(R_F + r_o)$. (5)

Substituting $i_i = i_s - i_f$ into equation (5) gives, after routine algebraic manipulation,

$$i_f = \frac{i_s}{\left\{1+\frac{(R_F+r_o)}{(r_p+r_i)}\right\}} \quad (6)$$

And,

$$i_i = \frac{i_s}{\left\{1+\frac{(r_p+r_i)}{(R_F+r_o)}\right\}} \quad (7)$$

Furthermore, $v_o = v_i - i_f R_F$ (8)

Thus from (6), (7),

$$v_0 = \frac{i_s r_i}{\left\{1+\frac{(r_p+r_i)}{R_F+r_o}\right\}} - \frac{i_s R_F}{\left\{1+\frac{(R_F+r_o)}{(r_p+r_i)}\right\}} \quad (9)$$

By design,$r_p \gg R_F \gg r_i, r_o$, so the first term in equation (9) can be ignored compared with the second and we can write,

$$v_0 \cong \frac{-i_s R_F}{\left\{1+\frac{R_F}{r_p}\right\}} \quad (10)$$

Or, in practice for DC and low frequency operation $v_o \cong -i_s R_F$, (11)

The quantity $\frac{(r_p+r_i)}{(R_F+r_o)}$ is identified as the loop gain taking into account the input and output resistances. A straightforward classical feedback approach ignores these. The input and output resistances with feedback are those without feedback reduced by the magnitude of the loop gain and are given by,

$$r_{if} = r_{of} \cong \frac{r_i R_F}{r_p}. \quad (12)$$

Consider now the frequency dependence of the trans-admittance. A cursory examination of Fig.1 using the method of 'Zero Value Time Constant Analysis' [13] suggests that a dominant time-constant might be $r_p C_o$, C_o being the capacitance at P, because all other nodal capacitances are of a similar order of magnitude but r_p is by far the greatest associated resistance. In that case, in terms of the complex frequency variable s,

$$Z_p(s) = \frac{r_p}{(1+sC_o r_p)} \quad (13)$$

Substituting this in place of r_p in equation (10) with the proviso $r_p \gg R_F$ finally gives,

$$Z_T(s) = \frac{v_o}{i_s}(s) = \frac{-R_F}{(1+sC_o R_F)} \quad (14)$$

The corresponding cut-off frequency, f_c is inversely related to R_F and is given by,

$$f_c = \frac{1}{(2\pi C_o R_F)} \quad (15)$$

3.Results

In a Cadence Simulation of Fig.1 the component choice was as follows: for all the Mosfets L=0.35µm; M_{22}-M_{27} and M_{29}-M_{32} had W=5µm; for the rest W=10µm. Operating conditions were $V_{DD} = -V_{ss} = 3.3V$ and I_1=I_2=10µA.

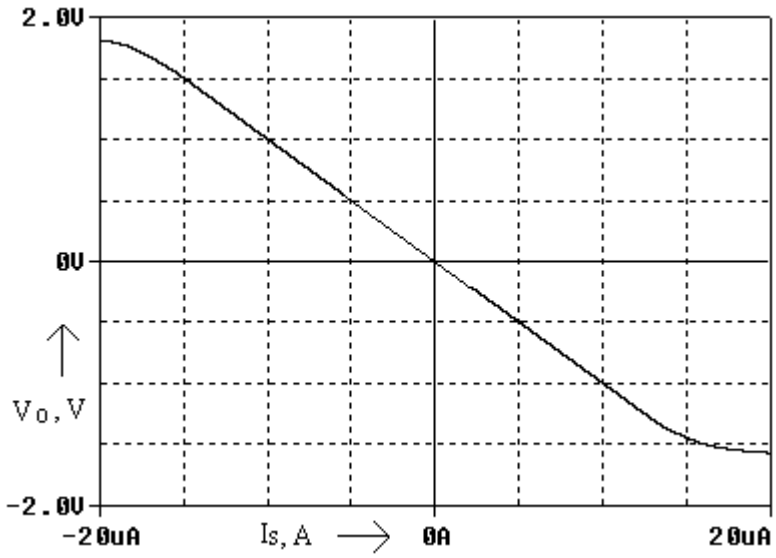

Fig.3a DC transfer characteristics of the proposed TIA for R_F=100kΩ

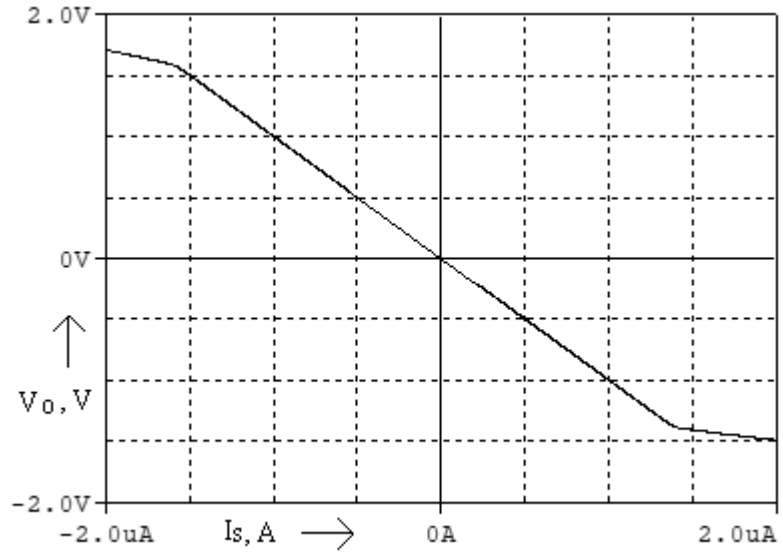

Fig.3b DC transfer characteristics of the proposed TIA for R_F=1MΩ.

Figs 3a,3b show, respectively, the DC transfer characteristics for R_F =100kΩ and R_F = 1MΩ. These resistances are chosen to give a guaranteed output voltage magnitude of 1V for I_S=10μA and I_S=1μA respectively. The graphs appear to be linear and pass through the origin (however, a separate check showed a 330μV offset from earth). For Vo>1.5V in Fig.3a there is non-linearity because of the onset of triode behaviour in the

P- channel RGC formed by M_{15}, M_{21} and M_{22}. There is also non-linearity for V< -1.25V, because of the onset of triode behaviour in the RGC formed from M_{20}, M_{27}, M_{28}.

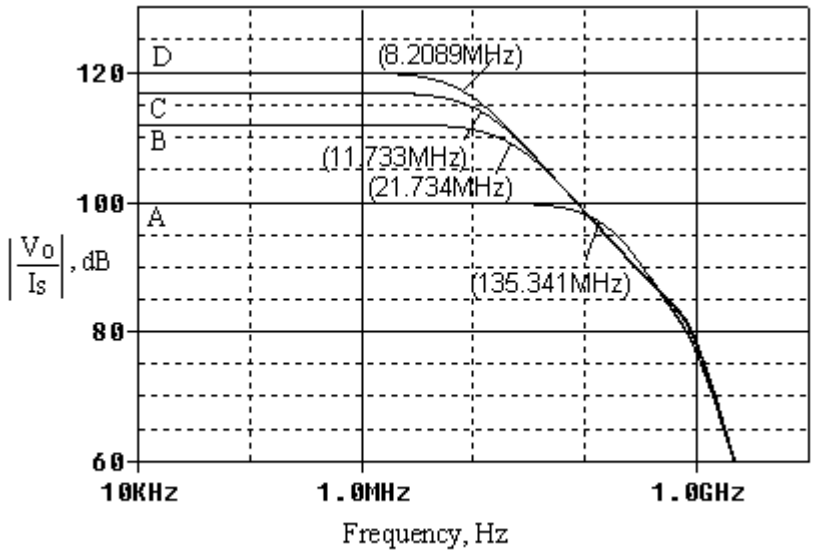

Fig.4a Frequency response plots A, B, C, D refer respectively to R_F = 100kΩ, 400kΩ,700kΩ and 1MΩ.

In the frequency response plots of Fig.4a, for non-optical current inputs the curves labelled A, B, C, D refer, here and henceforth, respectively, to R_F = 100kΩ, 400kΩ, 700kΩ, 1MΩ. The -3dB cut off-frequency, f_c, is shown by each curve. With R_F = 1MΩ (120dBΩ for a dB reference level of 1Ω), f_c= 8.209MHz: with R_F =700kΩ, f_c=11.73MHz compared with a value of 11.72 predicted from equation (15) for the same value of C_o. Similarly, for R_F = 400kΩ, f_c=21.734 compared with a predicted value of 20.52MHz, which is only 4.4% lower. However, equation (15) does not apply for 100kΩ itself. The break in the trade-off between gain and frequency response is because with high loop-gains, the frequency response is not controlled by a single dominant pole [14]. Other poles and a zero make their presence felt.

Stability is assured for R_F = 100kΩ for which the phase margin is 68˚, and is also for operation below 100kΩ. Thus, for R_F = 50kΩ, the phase margin is 51˚.

However, operation below R_F = 100kΩ is not recommended with input currents from photodiodes, as will be evident from the undesirable peak in the frequency response characteristics displayed below. The peak increases as R_F gets progressively smaller.

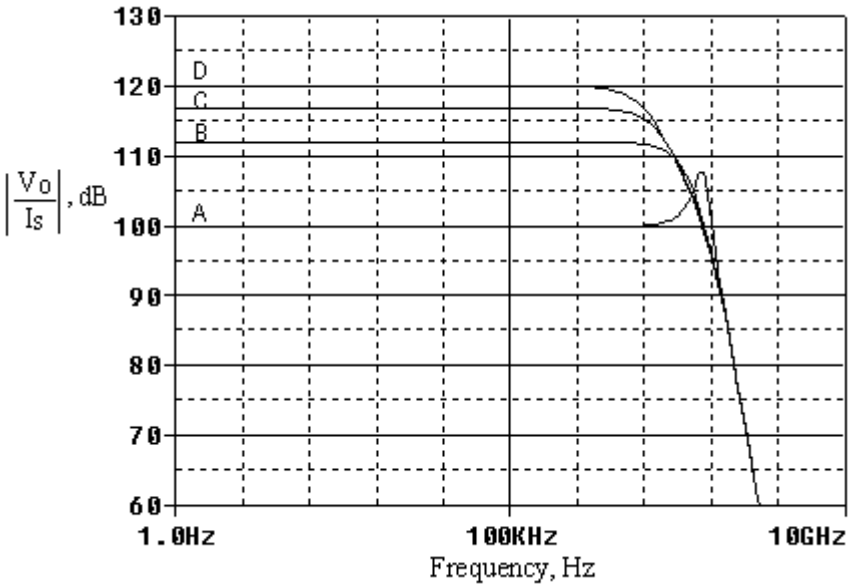

Fig.4b. Frequency response plots with photodiode junction capacitance of 0.5pF at the input and load capacitance of 0.1pF.

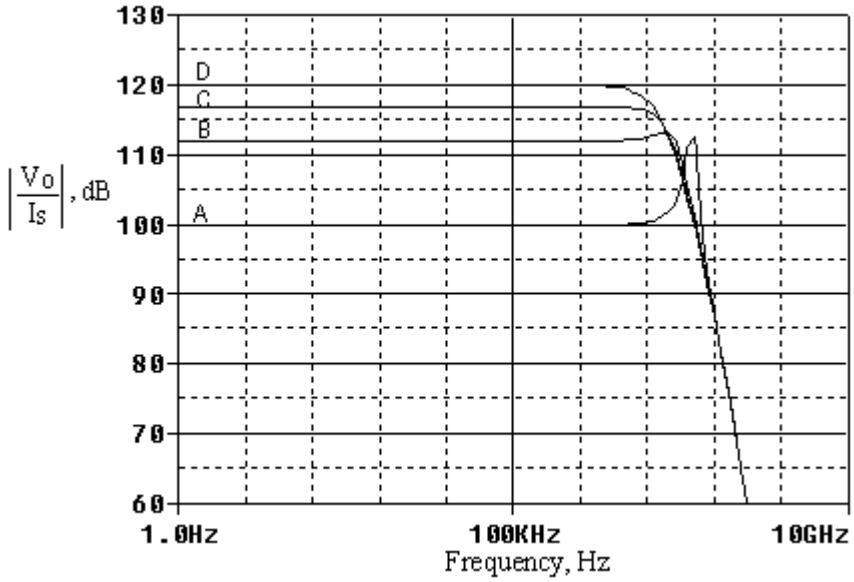

Fig.4c. Frequency response plots with photodiode junction capacitance of 2pF at the input and load capacitance of 0.1pF.

In Fig.4b, 4c, plots A, B, C, D refer respectively to resistance values mentioned earlier. The capacitance used refer to two types of photodiode junction capacitance. The 0.1pF refers to the likely load of a mosfet load in a succeeding stage.

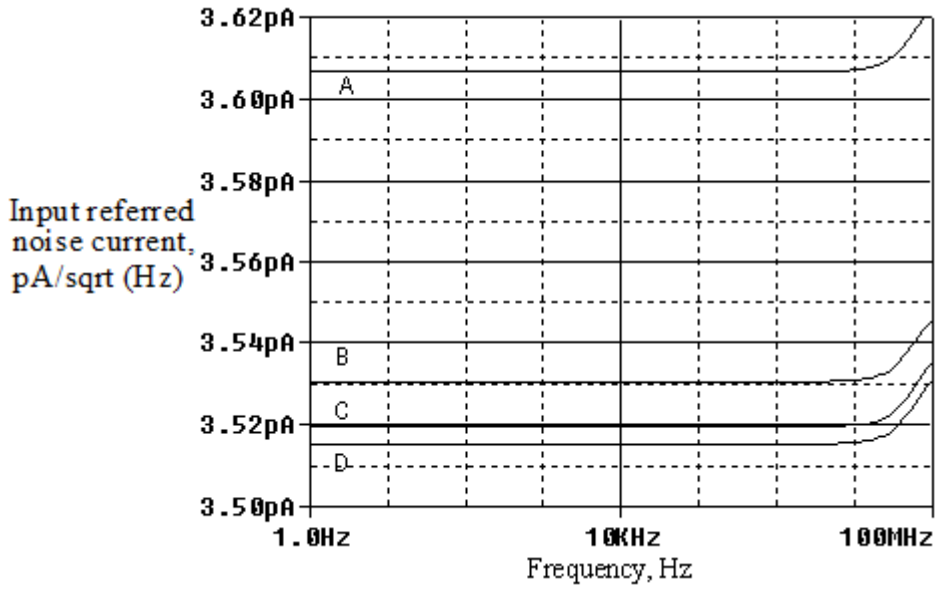

Fig.5 Input referred noise current (A/√Hz) of TIA with photodiode junction capacitance 2pF and load capacitance 0.1pF. The plots A, B, C, D refer respectively to R_F =100kΩ, 400kΩ, 700kΩ, and 1MΩ.

For frequencies below 10MHz, Fig.5 shows the input referred noise current which is the r.m.s output noise voltage divided by the TIA gain. In the proposed configuration the gain is high without feedback instability because the frequency response is dominated by a single pole. That is why the input referred noise current (3.5pA/√Hz) is significantly lower than that in the circuits described in [15].

Investigation showed that most of the noise occurred in the current mirrors [14], M_7, M_{21} and M_{14}, M_{28} of Fig.1. It can be reduced by operating with a lower bias current, e.g., with I_B = 5μA, the input referred noise current fell to 2.56pA/√Hz. However, operating with a lower I_B means a lower range of input currents that can be measured, without using a much higher value of R_F, and a higher input resistance.

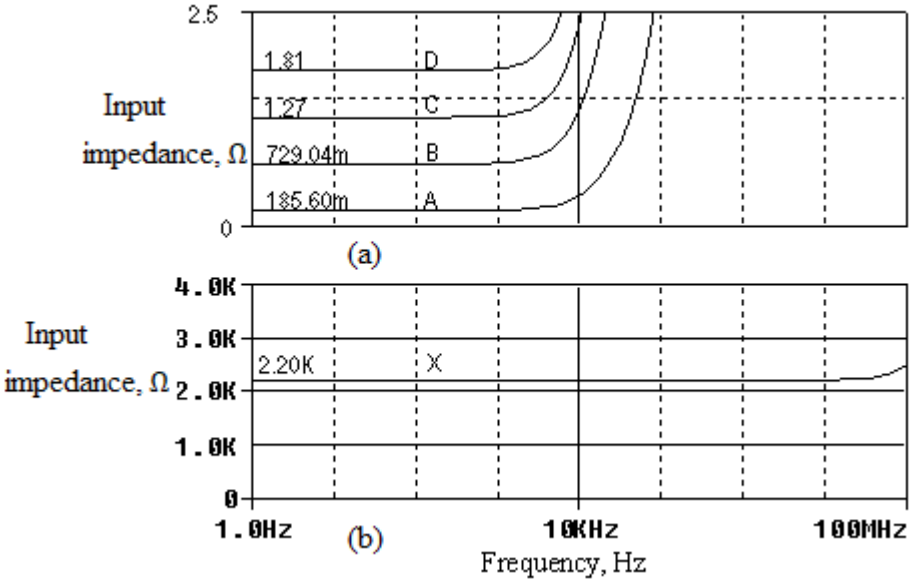

Fig.6 In (a) Plots A, B, C, D are input impedance plots with feedback resistors as mentioned earlier and in (b) plot X refer to input impedance without feedback resistor.

In Fig.6 the dramatic reduction in input impedance for each feedback resistance to less than 2Ω for curves A, B, C, D from its non-feedback value of more than 2kΩ in curve X is evidence of the very high loop-gain.

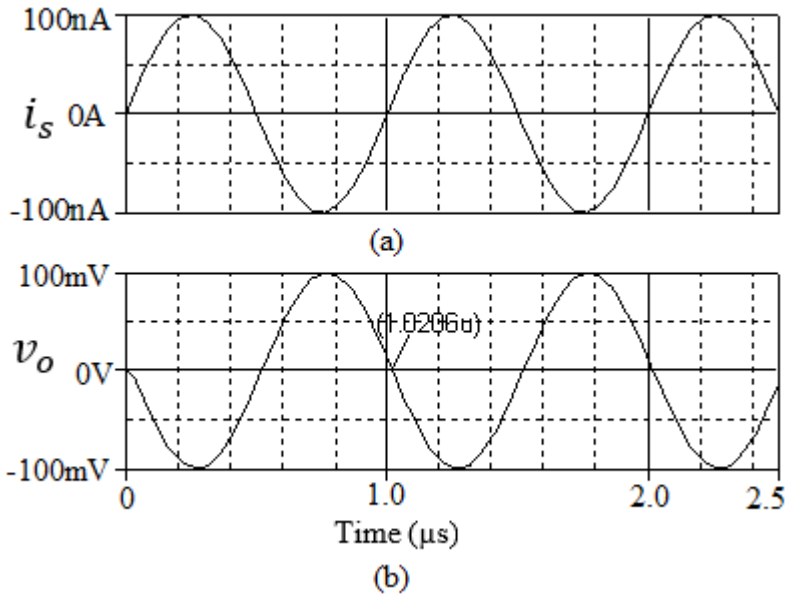

Fig.7 (a) Input signal, i_s (b) Output signal, v_o with R_F = 1MΩ.

As an illustration of the performance of the proposed TIA with a bidirectional current input, Fig.7 shows the output for a 1MHz, sinusoidal input with 100nA peak. In

this particular case there is an output delay of approximately 20nS. Table 1 shows the performance of the proposed circuit compared with that mentioned in [15].

Table 1 Performance comparison

Circuit characteristics	Proposed circuit		Shunt-feedback [15]	Current-mode [15]
Transimpedance	120dBΩ	100 dBΩ	112dBΩ	83dBΩ
Bandwidth	8.2MHz	135MHz	2MHz	115MHz
Input impedance	<2Ω	<0.2Ω	-	145Ω
Input-referred noise	*3.5pA/√Hz	*3.5pA/√Hz	185pA/√Hz	53nA/√Hz
Process Technology	0.35µm	0.35µm	0.18µm	0.18µm
Power Dissipation	330µW	330µW	0.5mW	28.6mW
*Reducible to 2.56pA/√Hz with I_B=5µA.				

Conclusions

A proposed low-current shunt-feedback transimpedance amplifier can be designed so that it does not require compensation components to ensure stability of the feedback loop because it uses only one high gain stage instead of the three lower gain stages of a conventional transimpedance amplifier. Cadence simulation results show very low input and output resistances, a high transimpedance gain and bandwidth that make it suitable for biosensing measurements.

Acknowledgements

The authors would like to thank the reviewers for their constructive comments.

References

[1]. Zheng, H., Ma, R., Liu, M., Zhu, Z. (2018). High Sensitivity and Wide Dynamic Range Analog Front-End Circuits for Pulsed TOF 4-D Imaging LADAR Receiver. *IEEE Sensors Journal*, 18(8),3114-3124.

[2]. Zheng, H., Ma, R., Liu, M., Zhu, Z. (2018). A Linear Dynamic Range Receiver with Timing Discrimination for Pulsed TOF Imaging LADAR Application. *IEEE Trans. on Instrumentation & Measurement*, 67(11), 2684-269.

[3]. Zheng, H., Ma, R., Zhu, Z. (2017). Design of Linear Dynamic Range and High Sensitivity Matrix Quadrant APDs ROIC for Position Sensitive Detector Application. *Microelectronics Journal*,63, 49-57.

[4]. Zheng, H., Ma, R., Zhu, Z. (2017). A Linear and Wide Dynamic Range Transimpedance Amplifier with Adaptive Gain Control Technique. *Analog Integrated Circuits and Signal Processing*, 90(1),217-226.

[5]. Ma, R., Zheng, H., Zhu, Z. (2017) A high sensitive 66 dB linear dynamic range receiver for 3-D laser radar. *Journal of Semiconductors*,38(8),81-86.

[6]. Damborsky, P., Svitel, J., Katrlík, J. (2016). *Essays in Biochemistry*, 60(1) 91-100; DOI: 10.1042/EBC20150010

[7]. Sackinger, E. (2010). The transimpedance limit, *IEEE Trans. Circuits Syst. I Reg. Papers*, 57(8), 1848-1856.

[8]. Sedra A., & Smith K. (2011). Chapter 9, International Student Edition, *Microelectronic Circuits*. (pp. 814 - 822). New York: Oxford University Press.

[9]. Ibrahim M., Levine P., Hirano, A. (2014). CMOS transimpedance amplifier for biosensor signals. *IEEE International Symposium on Circuits and Systems*, Melbourne VIC, Australia, June 2014, pp. 25-28., doi: 10.1109/ISCAS.2014.6865056

[10]. Park S. M., Toumazou C. (1997). Gigahertz low noise CMOS transimpedance amplifier. *Proceedings of IEEE International Symposium on Circuits and Systems,* 1, 209-212.

[11]. Ma, R., Liu, M., Zheng, H., Zhu, Z. (2018). A 77-dB Dynamic Range Low-Power Variable-Gain Transimpedance Amplifier for Linear LADAR. *IEEE Transactions on Circuits and Systems II: Express Briefs*. 65(2), 171-175.

[12]. Allen P.E., Holberg D. R. (2002). Chapter 4, Second Edition, *CMOS Analog Circuit Design* (pp. 141). New York: Oxford University Press.

[13]. Gray P.R., Hurst P. J., Lewis S. H., Meyer R. G. (2001). Chapter 7, Fifth Edition, *Analysis and Design of Analog Integrated Circuits* (pp. 518-527). U.S.A: John Wiley and Sons.

[14]. Sackinger, E., Guggenbuhl, W. (1990). A high swing, high impedance MOS cascode circuit. *IEEE Journal of Solid-State Circuits*, 25(1), 289-298.

[15]. Trabelsi, A., Boukadoum, M. (2012). A Comparative Overview of Two Transimpedance Amplifiers for Biosensing Applications. *IEEE International Symposium on Circuits and Systems*, 2227-2230.